ELSEVIER

Available online at www.sciencedirect.com

ScienceDirect

Procedia Manufacturing 49 (2020) 132–138

Procedia MANUFACTURING

www.elsevier.com/locate/procedia

8th International Conference on Through-Life Engineering Service – TESConf 2019, October 27 – 29, 2019

Inspection of electronic component using pulsed thermography

Lawrence Tinsley[a], Haochen Liu[a], Sri Addepalli[a], Wayne Lam[b], Yifan Zhao[a]*

[a]Through-life Egineering Services Centre, Cranfield Univerity, Cranfield, MK43 0AL, UK
[b]ITA Labs, The International Tin Association, St Albans, AL2 2DD, UK

* Corresponding author. Tel.: +44 (0)1234 754729; *E-mail address:* yifan.zhao@cranfield.ac.uk

Abstract

Counterfeit electronic components (CEC) are of great concern to governments and industry globally as they could lead to systems and mission failure, malfunctioning of safety critical systems, and reduced reliability of high-hazard assets. Depending on the cost of CEC going into the production line, some industries might look to have some sort of inspection capability in-house to screen critical components before they go to assembly. Although advanced counterfeit inspection methods have been developed for a variety of components, they generally exhibit a combination of disadvantages such as destructive, low throughput, high unit cost, or inaccessible to unskilled operator. This paper investigates the potential of pulsed thermography on detection of CEC in a fast and non-destructive manner. The second derivative of post-heat thermal response is used to construct a fingerprint to differentiate genuine and counterfeit components. Results successfully demonstrate the potential of the proposed solution.

© 2020 The Authors. Published by Elsevier B.V.
This is an open access article under the CC BY-NC-ND license (http://creativecommons.org/licenses/by-nc-nd/4.0/)
Peer-review under responsibility of the scientific committee of the 8th International Conference on Through-Life Engineering Service –TESConf 2019.

Keywords: Counteifeit detection; NDT; Correlation; TSR; Thermal signature

1. Introduction

Here Counterfeit electronic components (CEC), hidden trouble in electronic supply chain, are of great concern to governments, industries and defenses globally. They could cause catastrophic consequence or failure to critical in-services system due to its low-quality, low-efficiency or unreliability [1, 2]. Typical malfunctions of CECs such as overheating or short circuits, leading to fires, shocks or explosions that can result in serious injury and property crash in manufacturing, transporting and aviation. CECs also pose severe threats to cybersecurity, which has been identified as one of the most serious economic and national security challenges of the 21st century [3]. The legitimate electronic industries miss out on about $100 billion of global revenue every year because of counterfeiting, which is just one part of economic benefit in the murky CEC market [4]. Some stakeholders apply a variety of inspection methods to screen for counterfeits, but are limited by a combination of disadvantages [5]. For example; random spot checks are often

2351-9789 © 2020 The Authors. Published by Elsevier B.V.
This is an open access article under the CC BY-NC-ND license (http://creativecommons.org/licenses/by-nc-nd/4.0/)
Peer-review under responsibility of the scientific committee of the 8th International Conference on Through-Life Engineering Service – TESConf 2019.
10.1016/j.promfg.2020.07.008

time-consuming and can miss detections between inspections [6]. Other techniques, similarly, cannot be widely used due to features of destructive, low throughput, high unit-cost or over-sophisticated for unskilled operator [7]. Therefore, an intuitive, non-contact, high-efficient and low-cost non-destructive inspection technique is urgently demanded to reduce threaten of CECs.

Non-destructive testing (NDT) techniques have been widely used and play an important role in structure maintenance, degradation-assessment and though-life engineering [8-10]. Ranging from visual, eddy current, ultrasonic, magnetic particle, radiography to 3D tomography, thermography, multiple NDT methods show great applicability and competence in manufacturing, aviation, military and nuclear power industry. Among diversity of inspection methods, infrared thermography (IRT) is a powerful and promising technique due to the features of rapid, robust, non-contact inspection and intuitive images. IRT can be divided into two modes: active and passive. In order to rapidly identify counterfeit parts in batches, active thermography, which induce a heat flow into objects to generate thermal contrast and to highlight anomalies and defect, is more competent. Active thermography varies into different forms according to diversity of heat source including flash [11], laser [12], eddy current [13] and ultrasonic vibration. While the heating application differs between pulse, lock-in and modulated patterns, according the inspection requirement. The aims of this research is to develop a rapid, robust and non-destructive inspection technique for CECs. A high-energy pulse flash is applied to perform the pulse thermography test for electronic components.

In infrared thermography, thermal image processing methods are crucial to post-inspection process dealing with characteristic signal extraction, defect quantification to image quality improvement; for instance, the pulse phase thermography (PPT) algorithm [14] was one such method based on the phase signal of response of the thermal wave in inspected objects. But its capability is commonly limited in those cases whose initial decline frames is heavily impacted by noises. The Thermographic Signal Reconstruction (TSR) [15] method was a milestone algorithm which remarkably improved the spatial and temporal resolution of the thermogram sequence and consequently promoted the anomaly detectability. By focusing on thermal sequence reconstruction and alleviating the transient noise simultaneously, TSR-based analysis and corresponding developments have been applied on quantification of different defect information and transformation of the thermography data into RGB images [16, 17]. In addition, its theory has been extended to use with other algorithms, like Principal Component Thermography (PCT) [18]. The elegance of the TSR method has been demonstrated to be powerful at extracting subtle features in thermography data, which make it attractive for use in inspection of electronic components. The paper describes the experiment setup and TSR method used, detailing application of the TSR “fingerprint” method, followed by investigation of signature variation from experimental parameters, and between similar and different components, establishing a ‘base-line’ for minimum and maximum correlation, which is then compared with a real counterfeit example component.

2. Methodology

2.1. Experiment setup

In pulsed thermography, the experimental setup encompasses a short and high energy light pulse is projected onto the sample surface via flash lamps, shown in Fig. 1(a).

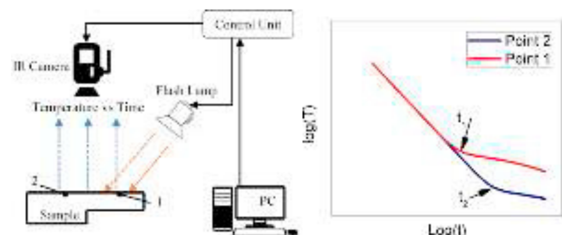

Fig. 1: (a) Experimental configuration of the pulsed thermographic inspection, where point 1 denotes a position on the sample surface with a reduced thickness and point 2 denotes a position representing the through-thickness; (b) Typical observed time-temperature decay curves in the logarithmic domain for the point 1 and 2, respectively.

Heat then conducts from the surface to the interior of the sample, leading to a continuous decrease of the surface temperature [1] (see Fig. 1(b)). An infrared camera captures the time-dependent response of the surface temperature. The time of cooling interruption can be used to estimate thickness (if thermal diffusivity is known) or diffusivity (if the thickness is known) of the sample material.

The experiments were conducted using the Thermoscope® II pulsed-active thermography system that comprises of two capacitor banks powered Xenon flash lamps mounted in an internally reflective hood and a desktop PC to capture and store data. A FLIR SC7000 series infrared (IR) radiometer operating between 3-5.1 µm and a spatial resolution of 640×512 pixels was used to perform the inspection. The samples were placed with their surface perpendicular to the IR camera’s line of sight at 250 mm from the lens. The flash energy applied was ~ 2 kJ over an inspection area of 250 mm × 200 mm. The pixel pitch is 0.32 mm.

Fig2. (a) shows a snapshot of the test board that includes various types electronic components. A raw temperature thermogram of the test board inspected from the top side from the first frame after flash is shown in Fig. 2(b).

2.2 Estimation of thermal fingerprint

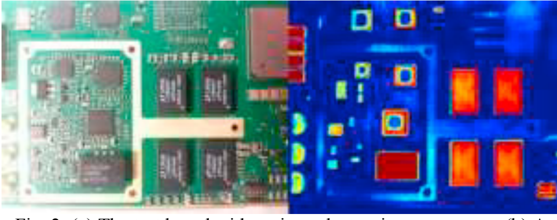

Fig. 2: (a) The test board with various electronic components; (b) A raw temperature thermogram of the test board; first frame after flash.

The surface temperature due to the back-wall at depth L for a homogeneous plate is given by [19]:

$$T(0,t) = \frac{Q}{\sqrt{\pi\rho c k t}}\left[1 + 2\sum_{n=1}^{\infty} R^n \exp\left(-\frac{n^2L^2}{\alpha t}\right)\right] \quad (1)$$

where $T(0,t)$ is the temperature variation of the surface at time t, Q is the pulse energy, ρ is the material density, c is the heat capacity, k is the thermal conductivity of the material, R is the thermal reflection coefficient of the air gap interface, and α is the thermal diffusivity.

A linear relation in the logarithmic domain with slope -0.5 as Eq. (2) exists for time and temperature if both sides of Eq. (1) are applied by the logarithmic operation [20].

$$\ln[T(t)] = \ln\left[\frac{Q}{\sqrt{\pi\rho c k t}}\right] - 0.5\ln(t) \quad (2)$$

The temperature response of any change in thermal material property from structure, damage or defect will derivate from the linear response. Shepard [21] proposed a Thermal Signal Reconstruction (TSR) technique to reduce temporal noise using a high order polynomial model to fit the temperature cooling curve. The model can be written as:

$$\ln[T(t)] = \sum_{i=0}^{N} a_i[\ln(t)]^i \quad (3)$$

where $T(t)$ is the surface temperature at time t, N is the model order, and a_i are coefficients to be estimated. Once the unknown coefficients a_i are estimated by the least square method, the temperature behaviour can be reconstructed to replace the raw data. The first and second derivatives of $\ln[T(t)]$ with respect to $\ln(t)$ can be calculated from the estimated coefficients directly, expressed as:

$$\frac{d\ln[T(t)]}{d\ln(t)} = \sum_{i=1}^{N} a_i \cdot i \cdot [\ln(t)]^{i-1} \quad (4)$$

$$\frac{d^2\ln[T(t)]}{d\ln^2(t)} = \sum_{i=2}^{N} a_i \cdot i \cdot (i-1) \cdot [\ln(t)]^{i-2} \quad (5)$$

The second derivative of temperature delay TSR fitting is used in this paper to construct the fingerprint. Fig. 3(a) plots an example for a single pixel on the selected region of interest. The first reason is that it is much more sensitive to the change of material, dimension or structure of component than the raw and first derivative. The byproduct is that it will be sensitive to noise as well, but the application of TSR could mitigate this potential problem. The second reason is that although the excitation heat applied on the surface is approximately uniform, there is still a variation of initial temperature across different regions. The raw temperature delay is not appropriate for pattern comparison directly because the initial applied temperature can be different even for the same component. The first and second derivatives are more appropriate because even the initial temperature is different, the change behaviour of temperature should be similar for two identical components. The fingerprint procedure can be summarised as follows:

1. Define the resolution of fingerprint, denoted by W x H.
2. Select the range of time in logarithmic domain $\ln(t) \in [x_{min}, x_{max}]$ and estimate the time step $\Delta\ln(t) = \frac{x_{max}-x_{min}}{W}$.

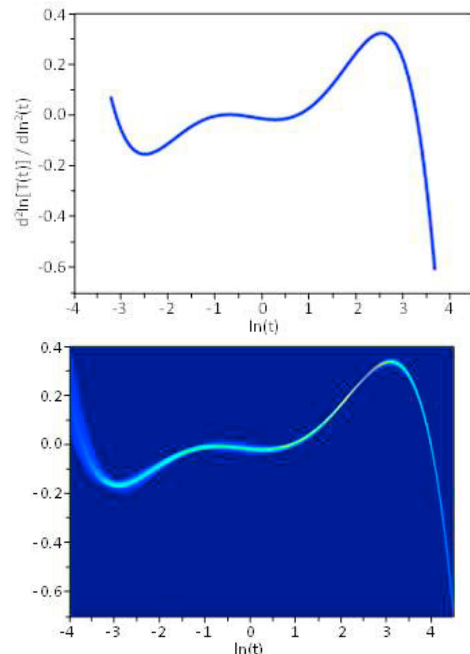

Fig. 3: (a) An example of the second derivative of TSR for a single pixel; (b) an example of the second derivative fingerprint for a selected region (multiple pixels).

3. For a pixel on the selected region, estimate the model shown in Eq. (3).
4. Calculate the value of the second derivative using Eq. (5) for $\ln(t) = \Delta\ln(t), 2\Delta\ln(t), \ldots, W\Delta\ln(t)$ and update the counter for the W x H bins by 1.
5. Repeat the step 3 and 4 for each pixel on the selected region and the fingerprint can be represented by the W x H bins.
6. Visualise the fingerprint, as shown in Fig.3 (b), where color represents the number of pixels in each bin.

2.3 Similarity of fingerprint

To differentiate whether a component is genuine or counterfeit, the fingerprint of the inspected component needs to be compared with that of the reference component. Methods are available to quantify the difference between two images, such as Mean Square Error (MSE), Peak Signal to Noise Ratio (PSNR) or Structural Similarity Index (SSIM) etc. In this paper, the 2nd differential correlation coefficient, r_{ab}, was employed to measure the similarity between two fingerprints: F_a and F_b, and it can be written as:

$$r_{ab} = \frac{\sum_{w=1}^{W}\sum_{h=1}^{H}(F_a(w,h)-\overline{F_a})(F_b(w,h)-\overline{F_b})}{\sqrt{(\sum_{w=1}^{W}\sum_{h=1}^{H}(F_a(w,h)-\overline{F_a})^2)(\sum_{w=1}^{W}\sum_{h=1}^{H}(F_b(w,h)-\overline{F_b})^2)}} \quad (6)$$

where $\overline{F_a}$ and $\overline{F_b}$ are the mean of the fingerprints F_a and F_b. The value of r_{ab} is always between 1 and -1. If the two fingerprints are similar, the value of r_{ab} is close to 1.

3. Results

3.1 Influence of flash power

The first step was to establish an appropriate flash power of the system for the study. Datasets were captured using four flash powers for the same part, using quarter values of the total flash power available to the system. The temperature decay profiles had contrasted origin and end-points, indicative of the different amount of heat energy input into the sample from the differing flash powers, while that of the 25% flash produced a weaker signal with a different shape compared to the other flash powers used. As can be seen by the temperature decay profiles from these tests, the data from 25% flash power produces a weaker, unreliable signal. The unusual shape of the 25% flash signal that is the source of the low correlation with the other results is likely to be related to poor polynomial fit of a noisier signal that would require more careful selection of polynomial fitting parameters to suppress it. Further analysis in the form of correlation of the 2nd differential fingerprints were made, to compare the similarity of the different flash powers, given in Table 1. The

Table 1. Cross-correlation analysis of fingerprint profiles from data captures of the same part taken at different flash heating powers.

	25%	50%	75%	100%
25%		0.12	0.11	0.12
50%	0.12		0.92	0.92
75%	0.11	0.92		0.93
100%	0.12	0.92	0.93	

Table 2. Cross-correlation between the fingerprints of 3 captures of the same part using the same parameters (part: W05)

	Test1	Test2	Test3
Test1		0.90	0.89
Test2	0.90		0.90
Test3	0.89	0.90	

Table 3. Cross-correlation of fingerprints: similar parts W01-W04

	W01	W02	W03	W04
W01		0.95	0.96	0.95
W02	0.95		0.96	0.95
W03	0.96	0.96		0.95
W04	0.95	0.95	0.95	

signal between 50-100% flash power exhibited a close correlation, indicating that each dataset produced a signal and respective fingerprint of similar quality. The full flash power was used as standard in further tests.

3.2 Repeatability for the same part

In order to gauge the significance of changes between any two fingerprints, it was important to assess the inherent variability in the data captures of the same component. One of the parts was captured on different occasions: two captures occurring hours apart, with other captures occurring between them, and one on a different day. This was to capture the inherent variability of the flash test in the data capture, and to measure the repeatability between the tests as a benchmark for the level of variation that can be expected. The correlation of the 2nd derivative fingerprints from these tests are shown in Table 2. The correlations between these repeat captures are high, which provides confidence in the repeatability between the captures and gives an early indication that any identified signatures could be reliably exploited. It should be noted that the correlation provided is a direct comparison of the 2nd derivative fingerprints, and only measure the gross variation between the captures. Making the assumption that four components on the board of the same type are identical; they are compared within the same capture providing a measure of variation within the same component in the same capture; suppressing the variability between captures, focusing on variation in the part, only. The correlations for these parts are shown in Table 3.

The strong correlations between the thermal signatures of these parts indicate that the four parts appear to have little

Table 4. Cross-correlation between fingerprints of the same part, W05 captured at two orientations perpendicular to each other, with the rotations also translated to the left and right of the field of view

	Normal	90º, left	90º, right
Normal		0.88	0.83
90º, left	0.88		0.90
90º, right	0.83	0.90	

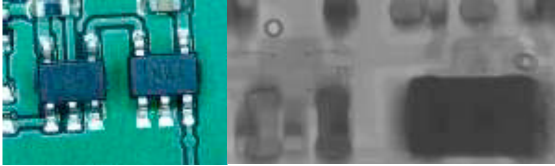

Fig. 4: (a) Visual inspection of parts W11 & W12; (b) x-ray inspection of W11 & W12, showing differences in internal wiring

differences between them, and, in comparison with the correlations in Table 2, where a different part was compared with multiple captures of itself, these differences indicate that there is likely to be a stronger variation between captures than there may be between parts, and that that features of the fingerprints, than just comparisons of the raw fingerprints. If any of the modules are counterfeit examples, their signals are more strongly correlated than a different part compares with other captures of itself; while this is not sufficient to conclude the modules are genuine, it at least strongly indicates that there is little difference between the four modules on the board. Further repeat captures were performed rotating the board by 90 degrees, and translating the component on the left, and the right of the field of view, in order to capture variation from the part's location in the field of view. The correlations between these are shown in Table 4.

The correlation factors for these are similar, but slightly lower than the repeat-captures of the same part (W05) presented in Table 2. This indicates that the location of the part within the field of view has a factor on the measured signal, and further highlights the importance of searching for features of the thermal signature to exploit, than simple comparisons of the part's signature as-measured.

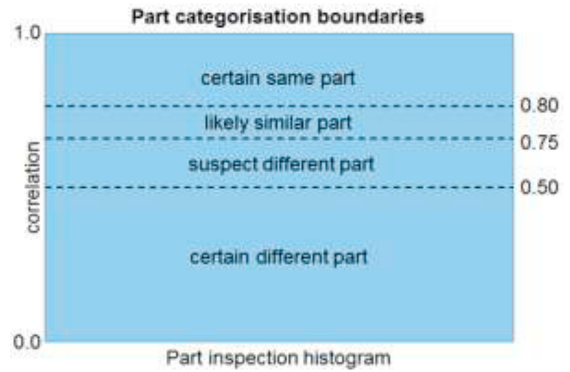

Fig. 5: Illustration of possible part condition categorisation boundaries, based on the proposed use of fingerprint analysis

3.3 Comparison of different parts

Enlightened by the comparisons of the same parts with repeat captures of themselves, and with comparisons of their twin parts of the same part model, the signatures of completely different parts were also compared; the correlations of these different components are provided in Table 5. As expected, the different parts exhibit measurably different signatures, providing much stronger differences in their correlations than demonstrated in the previous examples. This strong difference from different parts highlights thermography's capability for identification of parts using their internal material properties. Table 5 shows different parts, with 'same part' pairs, W07-W08, W09-W10, and W11, W12, which resulted in correlation coefficients of 0.84, 0.82, and 0.61, respectively. The W11-W12 matched pair were known to contain a suspect counterfeit part, confirmed by x-ray micrograph, as shown in Fig. 4. The fingerprint correlation coefficient between the counterfeit 'same part' pair, W11-W12 were higher than those produced by comparing the signatures of different parts, but lower than the repeat captures correlations of same parts, and were also

Table 5. Cross-correlation analysis of the fingerprints of different components with two matching pairs, one containing a counterfeit

	W01	W05	W07	W09	W13	W08	W10	W11	W12
W01		0.21	0.41	0.34	0.17	0.35	0.26	0.12	0.09
W05	0.21		0.51	0.24	0.40	0.59	0.24	0.32	0.34
W07	0.41	0.51		0.52	0.36	0.84	0.48	0.23	0.25
W09	0.34	0.24	0.52		0.12	0.43	0.82	0.10	0.08
W13	0.17	0.40	0.36	0.12		0.36	0.12	0.39	0.49
W08	0.35	0.59	0.84	0.43	0.36		0.41	0.23	0.27
W10	0.26	0.24	0.48	0.82	0.12	0.41		0.10	0.09
W11	0.12	0.32	0.23	0.10	0.39	0.23	0.10		0.61
W12	0.09	0.34	0.25	0.08	0.49	0.27	0.09	0.61	

lower than the correlations of same 'part pairs'. This result indicates that the TSR Fingerprint signature of a counterfeit part can be detectable with a rapid pulsed thermographic NDT inspection. The differences between the correlation coefficients for the different sample populations indicates that they could be used to produce classification boundaries based on their signature correlations, a sketch of which, based on these findings is shown in Fig. 5. It is expected that different parts and counterfeit types would exhibit different classification bands, which would require a large volume of part signatures to begin populating a usable classification database, which could be deployed on a user end system, implemented on a factory floor prior to the manufacture stage. The method could enhance detection screening for counterfeit proliferation, however its suitability would be limited to counterfeit methods which incur a change in thermal properties orientated normal to the surface.

4. Conclusions

The paper has demonstrated that pulsed thermography can be deployed to differentiate between genuine and counterfeit electronic components. The similarity of the proposed thermal fingerprint for the same part under different test environment, rotation angles is more than 0.8. The similarity of fingerprint of different parts is usually less than 0.5, suggesting that the TSR fingerprint has the potential to act a thermal-marker for detection of counterfeit electronic components. The ability of a counterfeit parts to produce a measurable difference in its thermographic signature would depend on the nature of the counterfeit of the part and its physical change of the part with respect to a genuine part, which would require further research with a larger volume with counterfeit components, to reinforce these findings.

Acknowledgements

This work was partly supported by the Lloyd's Register Foundation under Grant number GA\100113, and partly supported by the UK EPSRC Platform Grant: Through-life performance: From science to instrumentation (Grant number EP/P027121/1).

References

[1] H. Livingston, "Avoiding counterfeit electronic components," (in English), Ieee Transactions on Components and Packaging Technologies, vol. 30, no. 1, pp. 187-189, Mar 2007.
[2] J. Stradley and D. Karraker, "The electronic part supply chain and risks of counterfeit parts in defense applications," (in English), Ieee Transactions on Components and Packaging Technologies, vol. 29, no. 3, pp. 703-705, Sep 2006.
[3] U. Guin, K. Huang, D. DiMase, J. M. Carulli, M. Tehranipoor, and Y. Makris, "Counterfeit Integrated Circuits: A Rising Threat in the Global Semiconductor Supply Chain," (in English), Proceedings of the Ieee, vol. 102, no. 8, pp. 1207-1228, Aug 2014.
[4] M. Pecht and S. Tiku, "Bogus: electronic manufacturing and consumers confront a rising tide of counterfeit electronics," IEEE Spectrum, vol. 43, no. 5, pp. 37-46, 2006.
[5] U. Guin, D. DiMase, and M. Tehranipoor, "A Comprehensive Framework for Counterfeit Defect Coverage Analysis and Detection Assessment," (in English), Journal of Electronic Testing-Theory and Applications, vol. 30, no. 1, pp. 25-40, Feb 2014.
[6] U. Guin, D. Forte, and M. Tehranipoor, "Anti-Counterfeit Techniques: From Design to Resign," (in English), 2013 14th International Workshop on Microprocessor Test and Verification (Mtv): Common Challenges and Solutions, pp. 89-94, 2013.
[7] U. Guin and M. Tehranipoor, On Selection of Counterfeit IC Detection Methods. 2013.
[8] R. J. Ball and D. P. Almond, "The detection and measurement of impact damage in thick carbon fibre reinforced laminates by transient thermography," NDT & E International, vol. 31, no. 3, pp. 165-173, 1998/06/01/ 1998.
[9] M. S. Jadin and S. Taib, "Recent progress in diagnosing the reliability of electrical equipment by using infrared thermography," Infrared Physics & Technology, vol. 55, no. 4, pp. 236-245, 2012/07/01/ 2012.
[10] J. Mehnen, L. Tinsley, and R. Roy, "Automated in-service damage identification," CIRP Annals, vol. 63, no. 1, pp. 33-36, 2014/01/01/ 2014.
[11] S. M. Shepard, Advances in pulsed thermography (Aerospace/Defense Sensing, Simulation, and Controls). SPIE, 2001.
[12] H. C. Liu, C. X. Pei, J. X. Qiu, and Z. M. Chen, "Inspection of Delamination Defect in First Wall Panel of Tokamak Device by Using Laser Infrared Thermography Technique," (in English), Ieee Transactions on Plasma Science, vol. 46, no. 7, pp. 2699-2707, Jul 2018.
[13] G. Y. Tian, Y. L. Gao, K. J. Li, Y. Z. Wang, B. Gao, and Y. Z. He, "Eddy Current Pulsed Thermography with Different Excitation Configurations for Metallic Material and Defect Characterization," (in English), Sensors, vol. 16, no. 6, Jun 2016.
[14] X. Maldague and S. Marinetti, "Pulse phase infrared thermography," vol. 79, no. 5, pp. 2694-2698, 1996.
[15] S. M. Shepard and M. F. Beemer, Advances in thermographic signal reconstruction (SPIE Sensing Technology + Applications). SPIE, 2015.
[16] Y. F. Zhao, J. Mehnen, A. Sirikham, and R. Roy, "A novel defect depth measurement method based on Nonlinear System Identification for pulsed

thermographic inspection," (in English), Mechanical Systems and Signal Processing, vol. 85, pp. 382-395, Feb 15 2017.

[17] Y. F. Zhao, L. Tinsley, S. Addepalli, J. Mehnen, and R. Roy, "A coefficient clustering analysis for damage assessment of composites based on pulsed thermographic inspection," (in English), NDT & E International, vol. 83, pp. 59-67, Oct 2016.

[18] N. Rajic, "Principal component thermography for flaw contrast enhancement and flaw depth characterisation in composite structures," Composite Structures, vol. 58, no. 4, pp. 521-528, 2002/12/01/ 2002.

[19] S. K. Lau, D. P. Almond, and J. M. Milne, “A quantitative analysis of pulsed video thermography,” NDT E Int., vol. 24, no. 4, pp. 195–202, 1991.

[20] H. I. Ringermacher, R. J. A. Jr., and W. A. Veronesi, “Nondestructive Testing: Transient Depth Thermography,” US Patent No. 5711603, 1998.

[21] S. M. Shepard, “Reconstruction and enhancement of active thermographic image sequences,” Opt. Eng., vol. 42, no. 5, p. 1337, May 2003.